



**HAL**  
open science

## Entrained flow gasification of hardwood bark: experimental characterization of inorganic matter versus equilibrium and viscosity predictions

Françoise Defoort, Boris Grangier, Thierry Chataing, Serge Ravel, Gilles  
Ratel, Sylvie Valin

### ► To cite this version:

Françoise Defoort, Boris Grangier, Thierry Chataing, Serge Ravel, Gilles Ratel, et al.. Entrained flow gasification of hardwood bark: experimental characterization of inorganic matter versus equilibrium and viscosity predictions. *Energy & Fuels*, 2021, 35 (15), pp.12151-12164. 10.1021/acs.energyfuels.1c00993 . cea-04071672

**HAL Id: cea-04071672**

**<https://cea.hal.science/cea-04071672>**

Submitted on 17 Apr 2023

**HAL** is a multi-disciplinary open access archive for the deposit and dissemination of scientific research documents, whether they are published or not. The documents may come from teaching and research institutions in France or abroad, or from public or private research centers.

L'archive ouverte pluridisciplinaire **HAL**, est destinée au dépôt et à la diffusion de documents scientifiques de niveau recherche, publiés ou non, émanant des établissements d'enseignement et de recherche français ou étrangers, des laboratoires publics ou privés.

# Entrained flow gasification of hardwood bark: experimental characterization of inorganics matter versus equilibrium and viscosity predictions

*AUTHOR NAMES Françoise Defoort\*, Boris Grangier, Thierry Chataing, Serge Ravel, Gilles Ratel, Sylvie Valin.*

*AUTHOR ADDRESS* Université Grenoble Alpes (UGA), Commissariat à l’Energie Atomique et aux Energies Alternatives (CEA), Laboratoire d’Innovation pour les Technologies des Energies nouvelles et les Nanomatériaux (LITEN), DTCH, LRP, F-38000 Grenoble, France.

\*corresponding author’s email address : francoise.defoort@cea.fr

*KEYWORDS* Entrained flow reactor, Biomass ash, Gasification, Thermodynamic calculations, Viscosity calculations

*ABSTRACT* Hardwood bark (HW bark) containing a high ash yield (6.5 wt%) was gasified on a pilot scale in a pressurized entrained flow reactor (250 KWth) in allothermal conditions. Conventional physical-chemical characterizations were performed on the ash/slag (ash yield, weight and sieving, inductively coupled plasma, scanning electron microscopy with energy dispersive spectroscopy and X-ray diffractometry) and on the water (pH and Ionic Chromatography) both collected at the bottom of the entrained flow reactor (EFR). Simulations were performed to predict the phase speciation (solid + liquid + gas) at equilibrium with Factsage

7.3 and its databases and to predict the viscosity with the Factsage “melt” and Thomas models above and below liquidus temperature respectively.

Results showed that the inorganic matter collected could be characterized with a well closed overall and elemental mass balance. A slight pollution by the alumina wall of the reactor was observed. A very small amount (< 4%) of fly ash was noticed. The quench water was acidic due to the oxidation of the injected N<sub>2</sub> (and not due to N-biomass).

A good consistency was observed between experimental results of the main condensed phases and the prediction either from simple phase diagram or with global calculations but for only ¼ of the collected ashes. The remaining ashes - i.e. ¾ - contained unpredicted phases such as SiO<sub>2</sub> (from soil contaminant) and CaCO<sub>3</sub> (from raw HW bark) that did not react together. The viscosity was predicted to be between 1 to 10 Pa.s in the 1300 - 1400°C temperature range. This viscosity is below the 25 Pa.s criteria to have a slag flowing adequately along the EFR wall.

## **1. INTRODUCTION**

The gasification of coal in the entrained flow reactor (EFR) is currently used at industrial scale for heat, power, chemicals, gaseous or liquid fuels.<sup>1</sup> It is also recognized to be a promising technology for biomass.<sup>2</sup> The main advantages of EFR over other technologies such as those using fixed or fluidized beds are the possible extrapolation to large scale pressurized plants, the high gas quality (no tars) thanks to its high temperature (>1200°C), the high carbon conversion of the feedstock into carbon monoxide (and hydrogen) and a good management of the coal ashes. However, the application to biomass is also recognized as not being straightforward due to its problematic injection in the EFR and its different ash behavior compared to that of coal.<sup>2</sup> Both the ash-forming

elements and the ash yield of biomass are indeed very different from those of coal (Si-Ca-K-Mg-P and 0.1 to 20 wt% for biomass versus Si-Ca-Al-Fe-Na and 5 to 50 wt% for coal).<sup>3</sup>

The slagging EFR in which the ash forming components melt in the gasifier, then flow down the walls of the reactor, and finally leave the reactor as a liquid slag, is expected to be suitable for biomass due to the unavoidable presence of some amount of liquid in its ash.<sup>2,3</sup> There are two types of slagging reactors<sup>1</sup> – one with a hot ceramic insulated wall and another one with a water-cooled membrane wall. In the former, most of the ash deposited on the wall is liquid and wear the ceramic by chemical corrosion (dissolution) and erosion (spalling). The latter is working as a self-crucible thanks to the formation of a protective layer of a solidified slag. The hot wall reactor is more prone to low ash yield feedstocks to limit the interaction with the ceramic wall, unlike the water-cooled membrane wall reactor in which a sufficient amount of ash is necessary to make the self-crucible layer.<sup>1</sup> In both cases, the properties of the liquid ashes (melting temperature, viscosity) are important to avoid clogging the outlet of the gasification chamber, dissolving the ceramic of the hot wall reactor or disorganizing the protective layer of the solidified slag of the water-cooled membrane wall reactor.

The ash properties and behavior of biomass in slagging EFR gasification is thus an important feature to be studied and is the purpose of this paper.

Slagging gasification of coal has been studied for a long time on laboratory, pilot and plant scales. It is known to require a fluxing material such as limestone in order to obtain the adequate properties of the slag at reasonable temperatures.<sup>1</sup> Biomass studies in EFR-like conditions - i.e. fast pyrolysis - are quite numerous on a laboratory scale in a drop tube furnace to study the carbon conversion to syngas but there are few studies of the ash behavior<sup>4,5,6,7,8,9,10</sup> and even less on the pilot scale.<sup>11,12,13,14,15</sup> Autothermal reactors are commonly used on a pilot scale but no allothermic

reactor has ever been studied on a pilot scale for biomass in our knowledge nor to a working pressure of 5 bars. In the former case, a part of the biomass is burned in the O<sub>2</sub> flame to provide heat to the reactor and to ensure the endothermic gasification reaction. In the latter case, external energy is supplied to the reactor. When this external energy is for example electrical, it is necessary to add some oxidized agents (H<sub>2</sub>O, CO<sub>2</sub> or O<sub>2</sub>) otherwise the conditions are pyrolysis. Another solution is to bring external energy by a natural gas/O<sub>2</sub> burner. In this case, the products of the exothermal reaction (from the natural gas burner or fraction of biomass burned) are CO<sub>2</sub> and H<sub>2</sub>O that are in enough amount to allow gasification conditions. Allothermic conditions allow to maximize the conversion of carbon from biomass to synthesis gas (CO, H<sub>2</sub>). The purpose of this study is to focus on the slag behavior of biomass on a pilot scale in an allothermal way using a natural gas/O<sub>2</sub> burner at a working pressure of 5 bars.

For instance, some authors have studied - on a laboratory scale - the behavior of the ashes of certain biomasses such as wood with a low ash yield<sup>4</sup> and different types of straw<sup>5,6</sup> supported by thermodynamic equilibrium calculations. A small amount of liquid with some solid CaO particles were observed for wood with a low ash yield at temperatures as high as 1450°C.<sup>4</sup>

Most of the authors using a pilot scale have studied the slag behavior of woody biomass in a hot wall reactor at a medium total pressure (2 bars)<sup>11,13</sup> or at higher total pressure (7 bars)<sup>12</sup>. Temperatures were from 1050 to 1500°C. The slags were studied from specific sampling taken along the wall at the bottom colder zone of the reactor (1050 to 1200°C) or from slag collected in the quench pool or the reactor outlet. The main finding was the influence of SiO<sub>2</sub>-feldspar rich soil contaminant on woody biomass to generate slag that was otherwise absent or in very low amounts in the same temperature range.<sup>11</sup> Another study performed at higher pressure (7 bars) at 1200-1320°C confirmed the effect of adding silica (from a peat resource) to a clean soil-free woody

biomass on the flow ability of the slag and on the interaction with the alumino-silicate wall.<sup>12</sup> An important finding of the Carlsson<sup>13</sup> study is the drastic blocking of the reactor outlet when the temperature was increased from 1250-1350 to 1450-1500°C. Yet the initial clean woody biomass had very little ash yield (0.35 wt%) with very low theoretical ash introduced in the reactor (less than 500 g). The reason proposed was a drastic higher content of liquid slag, resulting from the interaction of the alumino-silicate wall with the gaseous KOH species and/or condensed ash. The author's interpretation was supported by slag characterization, thermodynamic equilibrium and viscosity calculations.

Very few results were published using biomass on a pilot scale in the configuration of a cold wall reactor. They mostly investigated the thermophysical and chemical properties of real slags collected after testing<sup>14</sup> and studied the slag thickness and deposition rate on the cooled membrane.<sup>15</sup> The feedstocks were slurries derived from low ash yield biomass (< 5 wt%), for instance charcoal from wood and straw pyrolysis, in the Bioliq demonstration plant<sup>16</sup>

The objective of this work is therefore to present the behavior of the slag of a hardwood bark (HW bark) biomass containing a high ash yield (6.5 wt% at 815°C) gasified on a pilot scale hot wall pressurized EFR (250 kWth). Furthermore, an overall and elemental mass balance of the inorganic matter could be achieved, which is rarely performed in literature. Conventional physico-chemical characterization - scanning electron microscopy with energy dispersive spectroscopy (SEM-EDS) and powder X-ray diffractometry (P-XRD) - of the ash/slag were performed along with thermodynamic equilibrium simulations and viscosity calculations.

This work was done within the frame of the H2020 Pulp&Fuel project involving ten partners from four European countries. This project received funding from the European Union's Horizon 2020 research and innovation program. It addresses the thermochemical conversion of industrial wastes

produced at a pulp and paper mill into biofuel. The project aims at improving gasification performance through dry gasification experiments from dry resources such as bark (with fixed bed and entrained flow reactors), and supercritical water gasification from wet resources such as black liquor.

## 2. MATERIALS AND METHODS

### 2.1 Feedstock

The Hardwood bark (HW bark) was provided by Fibre Excellence Saint-Gaudens (one of the partners in the Pulp&Fuel project in France). It was chosen because it is a “waste” resource coming from the paper industry and not used in the paper production process. It was grinded and sieved with 600 µm and 300 µm meshes to eliminate large particles and to reduce the fine particle fraction to reach adequate feeding properties for an EFR. A cold injection test with the powder confirmed its ability to be injected in the gasifier. This sieving process caused a significant weight loss of raw material. The mass yield is 30 wt%, which means that 70 wt% of the initial powder could not be used.

The composition after grinding and sieving is shown in **Table 1**.

Its composition and lower heating value (LHV) is typical of woody biomass, and its ash yield of 6.5 wt% typical of bark.<sup>3</sup> The main oxides are SiO<sub>2</sub>-CaO-K<sub>2</sub>O with SiO<sub>2</sub> being the highest contrary to woody biomass usually CaO richer.<sup>3</sup> Furthermore, Al<sub>2</sub>O<sub>3</sub> is also quite high for a woody biomass, indicating a probable slight soil pollution.



	HW bark
Moisture (wt% ar*)	9.0
LHV* (MJ/kg)	17.8
	In wt% db*
Ash (815°C)	6.5
C	49.2
H	5.63
N	0.35
S	0.03
Cl	0.025
O (by difference)	37
	In mg/kg db*
Al	1690
Ca	15174
Fe	976
Mg	866

Mn	238
P	329
K	2728
Si	12476
Na	316
Ti	76
Pb	2
Zn	60
	in wt% ash calculated
SiO <sub>2</sub>	45.7
CaO	36.4
Al <sub>2</sub> O <sub>3</sub>	5.5
K <sub>2</sub> O	5.6
Na <sub>2</sub> O	0.7
MgO	2.5
Fe <sub>2</sub> O <sub>3</sub>	2.4

P <sub>2</sub> O <sub>5</sub>	1.3
-------------------------------	-----

**Table 1.** Composition and characteristics of the feedstock introduced

\* LHV: Lower Heating Value

db: dry biomass

ar: as received

## **2.2 Entrained flow reactor**

The GIROFLE entrained flow reactor is a hot wall slagging reactor designed to be able to gasify up to 50 kg/h of biomass at 1500°C, at a total pressure of 30 bars (<http://www.cea.fr/cea-tech/liten/genepi/en/Pages/equipements/girofle.aspx>). A scheme of the facility is shown in **Figure**

**1.**

The reactor is heated with a gas burner (maximum power: 150 kW) fed with natural gas and pure O<sub>2</sub>. The external vessel is cooled by cold water flowing into a coiled tube welded onto its outer surface.

The pressure inside the reactor is regulated with valves situated on the exit line. It is measured at different locations of the facility and in particular at the top of the reactor.

The biomass is stored in two identical lock hoppers of 100 litres each containing up to about 20 kg of fine powder. A dosing screw controls its feeding rate. The biomass is fed at the top of the gasifier. N<sub>2</sub> is injected in the biomass feeding system to avoid hot gas backflow and to assist biomass flow. The solid feeding line ends up at the top of the reactor with a solid injection tube, vertically placed next to the burner and cooled in a double jacket (annular zone cone) by the circulation of neutral gas (N<sub>2</sub> optionally mixed with helium or argon) even when biomass has not yet been injected.

An alumina tube of 0.25 m in diameter and 0.014 m in thickness delimits the internal part of the reactor. Refractory bricks (0.23 m thick) made of  $\text{Al}_2\text{O}_3$  and  $\text{SiO}_2$  surround this tube. These bricks ensure the thermal insulation. The internal part of the reactor is divided in two parts. The upper part (about 1 m long) is heated by the burner and constitutes the reactive zone. The lower part is the quench zone, which can be cooled either by deionized water, or by  $\text{N}_2$ , in both cases with three nozzles located at the same level.

The height between the top of the quench zone and the lateral exit of the gas is about 1.25 m. The gas then flows into a heat exchanger in which water is condensed, and through filters before being burnt in a post-combustion unit.

The bottom of the reactor is filled with deionized water, whose level is regulated all along the experiment. Slags made of biomass ash are solidified when falling in this water.

Thermocouples are positioned at eleven levels in the reactor. For each level, several thermocouples are distributed radially from the cooled vessel to the internal alumina wall. For the analysis of experimental results, we are going to consider the measurements of the thermocouples situated near to the internal wall of the reactor as their values are the closest to the gas and biomass temperature.

A constant  $\text{N}_2$  flowrate is introduced in the reactor as a protection gas for the windows and in an annular space outside the internal reactor.

The total dry gas flowrate is measured after the heat exchanger with a Coriolis mass flowmeter. Moreover, helium as a tracer gas is introduced with a controlled flowrate on the exit line before the heat exchanger.

Gas composition is analyzed by a micro-gas chromatograph ( $\mu$ GC) which allows quantifying the volume content of the gas species coming from gasification ( $H_2$ ,  $CO$ ,  $CO_2$ ,  $CH_4$ ,  $C_2H_4$ ,  $C_2H_6$ ,  $C_2H_2$ ,  $C_3H_8$ ,  $C_6H_6$ ,  $C_7H_8$ ,  $H_2S$ ,  $COS\dots$ ) and of the injected gas species ( $O_2$ ,  $He$ ,  $N_2$ ). One analysis is performed every three minutes.

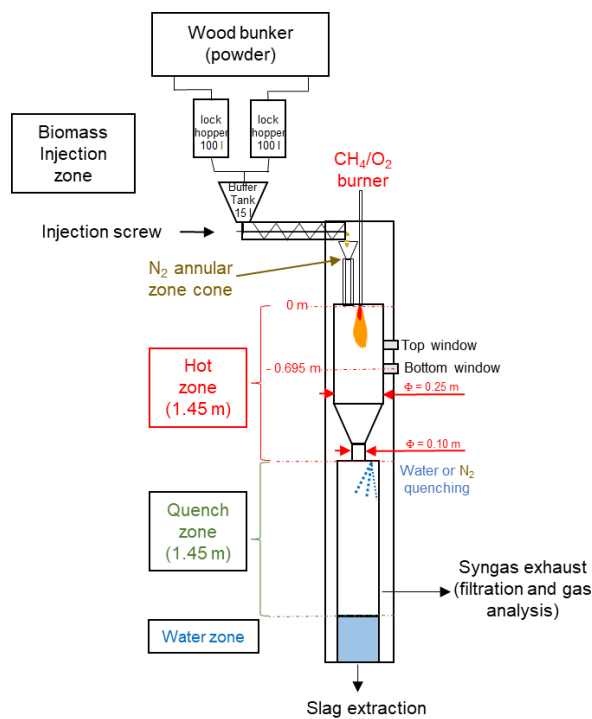


**Figure 1.** Scheme of the entrained flow reactor facility

### 2.3 Experimental procedure

The days before the day of the experiment, the reactor is first-preheated up to more than  $700^{\circ}C$  thanks to natural gas combustion in the burner, with a reactor pressure of 2 bars. Then, the pressure in the reactor is very progressively increased up to the target value, keeping the same combustion power.

On the day of the experiment, the burner power is adjusted to reach the target temperature of the test. When biomass starts to be fed, the burner power is first increased and then stabilized to keep the target temperature in the reactor.

## **2.4 Characterization of residues**

After the test, the bottom of the reactor was opened in order to recover the water and the solid residues. The collected residues were dried, weighted and sieved with several mesh sizes (100, 630 and 2500  $\mu\text{m}$ ). The first two approximately corresponded to the initial biomass particle size.

Several analysis were performed in each class of residue:

- Weighing
- Measurement of ash yield at 815°C. The complement to this ash yield is estimated to be the unburned carbon.
- Chemical composition measured by inductively coupled plasma spectrometry (ICP)
- Presence of amorphous and crystalline phases analyzed by powder X-ray diffraction (PXRD). A D8 Bruker Advance apparatus with Cu  $K_{\alpha}$  radiation (40 kV and 30 mA) equipped with a fast Lynxeye detector was used. The samples were ground to the consistency of a fine flour if necessary. Approximately 0.5 g of ash was placed in an amorphous silica sample holder and flattened with a microscopy glass. Diffractograms were obtained over a  $2\theta$  interval between 10° and 70°. Phase analysis was performed with DIFFRAC Plus/EVA software using the International Centre for Diffraction Data (ICDD) database PDF-4.

Some slag samples were analyzed by scanning electron microscopy (SEM) coupled with energy-dispersive X-ray spectroscopy (EDS) for morphology and elemental composition (semi-quantitative) of the observed phases. The instrument used was a Philips XL30 SEM coupled with

an Oxford Instruments EDX system (INCA software). The slags were embedded under vacuum in epoxy resin and polished with water-free lubricants. The samples were coated with graphite to make them conductive, allowing for SEM analysis.

The water collected at the bottom of the EFR reactor was weighed and analyzed by pH-metry and ionic chromatography (IC) to obtain their anions and cations.

## **2.5 Simulation tools**

### **2.5.1 Thermodynamic calculations**

The thermodynamic calculations were performed by minimization of the Gibbs free energy of the total system with the Factsage software 7.3 and adequate databases.<sup>17</sup> The compounds database FactPS for the gas phase and FToxid database for the oxide solid and liquid solution phases were used. They are used to predict all phases (solid + liquid + gas) at equilibrium at any temperature and any total pressure. The software allows to take into account all solid and liquid solutions in the calculations. For some of them the user has to choose. The complete list of these solutions is reported in the **Supporting information (Table S1)**. The main solutions found at equilibrium are the liquid solution (SLAGA) and the solid solutions (KASH, WOLLA, LEU1, OlivA, Mel, Feld).

The condensed phases at equilibrium were calculated firstly using a simplified method consisting in a ternary phase diagram with the three main oxides of the feedstock ashes ( $\text{SiO}_2\text{-CaO-K}_2\text{O}$ ). Secondly using the “equilib” module referred as global calculations, taking into account the atmosphere, the total pressure and all the elements of the feedstock. This allowed to take into account the inorganic volatilities and to simulate the inorganic fractionation between the gas and the condensed phases. The initial inputs were the quantities of gas from the burner ( $\text{O}_2$ ,  $\text{CH}_4$ ) and those of the neutral gas introduced ( $\text{N}_2$ ) perkg/h of HW bark introduced (**Supporting information**

available Table S2 to S4). The total pressure was 5 bars and the temperature was varied between 800 and 2000°C. The results of the condensed phases were plotted in grams per kg of dry biomass. The volatilization of each element was plotted in grams per introduced gram (or mols per introduced mol).

Some calculations were also performed taking into account the ceramic refractory wall material interaction with the ashes, i.e. dense alumina in the upper part and refractory concrete (60% Al<sub>2</sub>O<sub>3</sub>-40% SiO<sub>2</sub>) in the lower conical part. The temperature of 1150°C was chosen because it is close to the one measured in the lower part of the refractories next to the cone (**Figure 2**). The input data were the same mass balance (1 kg biomass + atmosphere) as previously but adding a small amount of each kind of refractory. A maximal mass of 20 g was chosen because it corresponds to an ablated refractory crown estimated about 0.001 m in depth and 0.02 m high in the conical part of the reactor ( $3.14 \cdot 0.1 \cdot 0.02 \cdot 0.001 \cdot 3.2$  with refractory density = 3.2 g/10<sup>-6</sup> m<sup>3</sup>).

### **2.5.2 Viscosity calculations**

Viscosity of the liquid slags can be predicted thanks to simple models (like in Seiler<sup>18</sup> with the Urbain model<sup>19</sup>) or more sophisticated models taking into account the structure of the liquid phase.<sup>20,21,22</sup>

In this report we calculated the viscosity of the slag using the Factsage model “melt”.<sup>20</sup>

Below the liquidus temperature, a solid fraction is appearing and drastically increases the viscosity. The model of Thomas<sup>23</sup> was used to calculate the apparent viscosity of this semi-solid mixture. This model was established for hydrodynamic suspensions, so there is no certainty about their relevance in the case of ash. Other models exist,<sup>24</sup> however, they involve parameters whose



physical meaning is not always well defined or which are not known in the case of suspensions formed by a mixture in the course of solidification.

The semi solid viscosity  $\eta_{\text{semi solid}}$  is therefore calculated using the Thomas formula (eq. 1):

$$\eta_{\text{semi solid}} = \eta_{\text{liq}} \cdot [1 + 2.5 f_{\text{vs}} + 10.05 f_{\text{vs}}^2 + 0.00273 \cdot \exp(16.6 \cdot f_{\text{vs}})] \quad (\text{eq.1})$$

where  $\eta_{\text{liq}}$  is the viscosity of the liquid phase in equilibrium

- $f_{\text{vs}}$  is the solid volume fraction.

The solid volume fraction  $f_{\text{vs}}$  is calculated from the volumes occupied by each phase  $v_{\text{solid}}$  and  $v_{\text{liquid}}$  (eq.2):

$$f_{\text{vs}} = (\sum v_{\text{solid}}) / (\sum v_{\text{solid}} + \sum v_{\text{liquid}}) \quad (\text{eq.2})$$

with  $v_{\text{solid}} = m_{\text{solid}} / d_{\text{solid}}$

$$v_{\text{liquid}} = m_{\text{liquid}} / d_{\text{liquid}}$$

The volume of the phases  $v_{\text{solid}}$  and  $v_{\text{liquid}}$  were calculated from their density and from the mass calculated by Factsage ( $m_{\text{solid}}$  and  $m_{\text{liquid}} = m_{\text{SLAGA}}$ ):

The density of the liquid phase  $d_{\text{liquid}}$  is estimated by the additivity rule of molar mass and molar volume of the oxides constituting the liquid phase (in molar fraction) (eq.3)

$$d_{\text{liquid}} = (\sum_{\text{iox}} X_{\text{iox}} M_{\text{iox}}) / [(1 + 0.0001 (T_{\text{slag}} - 1773)) \cdot (\sum_{\text{iox}} X_{\text{iox}} V_{\text{iox}})] \quad (\text{eq.3})$$

with  $X_{\text{iox}}$  = the oxides of the liquid phase ( $\text{SiO}_2$ ,  $\text{CaO}$ , etc)

$$M_{\text{iox}} = \text{the molar mass of oxide}$$

$V_{iox}$  = the molar volume of oxide in its liquid state at 1773 K (**Table 2**). The temperature coefficient ( $dV/dT$ ) is assumed to be 0.01% per Kelvin for each one<sup>25</sup>

$X_{iox}$  = the molar fraction of oxide of the liquid phase SLAGA. This quantity is not given by the software and must be calculated for example from the elemental molar composition of SLAGA (Mol-i\_FToxid-SLAGA)

iox	$M_{iox}$ (g/mol)	$V_{iox}$ (1773K) ( $10^{-6}$ m <sup>3</sup> /mol)
Fe <sub>2</sub> O <sub>3</sub>	159.68	38.4 <sup>a</sup>
FeO	71.84	15.8 <sup>a</sup>
CaO	56	20.7 <sup>a</sup>
K <sub>2</sub> O	94.2	47.28 <sup>b</sup>
SiO <sub>2</sub>	60.08	26.86 <sup>b</sup>
Al <sub>2</sub> O <sub>3</sub>	101.96	37.42 <sup>b</sup>
MgO	40.3	16.1 <sup>a</sup>
Na <sub>2</sub> O	62	33 <sup>a</sup>

**Table 2.** Molar mass and liquid molar volume at 1773K of oxides with their references (<sup>a</sup>:

<sup>25</sup> and <sup>b</sup>: 26)

The density of the solid phases  $d_{\text{solid}}$  are reported in **Table 3**. Several solid phases are calculated to be in equilibrium with the liquid phase. Only the main ones were taken into account. No effect of thermal expansion was taken into account.

	$d_{\text{solid}}$ (g/10 <sup>-6</sup> m <sup>3</sup> )
WOLLA (CaSiO <sub>3</sub> )	2.90
Ca <sub>3</sub> MgSi <sub>2</sub> O <sub>8</sub>	3.34
OlivA (Ca,Mg,Fe) <sub>2</sub> SiO <sub>4</sub> )	3.3
KASH (KAlSiO <sub>4</sub> )~ LEU1 (KAlSi <sub>2</sub> O <sub>6</sub> )	2.5

**Table 3.** Density of the solid phase (Factsage)

### 3. RESULTS AND DISCUSSION

#### 3.1 Progress of the test, process temperatures and syngas

Conditions of the tests are shown in **Table 4**. The injection of HW bark powder was stable during 5 hours with a powder flow rate of 6 kg/h corresponding to 30 kg injected, a total pressure of 5 bars and a burner power of 33 kW in order to be in an allothermal mode. The oxidant (O<sub>2</sub>) brought into the system comes from the natural gas burner, and straightly reacts with the natural gas. The Equivalent Ratio associated to natural gas (ER<sub>nat-gas</sub>) is 1.0. However, a global Equivalent Ratio (ER<sub>global</sub>) considering all combustible species (natural gas and biomass) can also be calculated: ER<sub>global</sub>=0.55.

The water quench was injected as a water spray at the reactive zone exit to cool down gases and ashes:

	Test conditions
Test duration	4h42
Biomass flow rate (total input mass)	6.13 kg/h (30.355 kg ar *)
Total pressure	5 bars
Burner power	33 kW
Natural gas (CH <sub>4</sub> )	3.4 Nm <sup>3</sup> /h

O <sub>2</sub>	6.8 Nm <sup>3</sup> /h
N <sub>2</sub>	7.53 Nm <sup>3</sup> /h
Water quench	6.5 liter/h
Mean wall temperature between 0 and -0.435 m	1280-1330°C

**Table 4.** Stabilized conditions of the test (\* ar: as received)

The temperatures (**Figure 2**), gas analyses and combustion power of the burner (**Figure 3**) measured show that the gasification was stable all along the test. No blockage linked to the ash management was observed during the test even if about 1.8 kg theoretical ashes were injected.

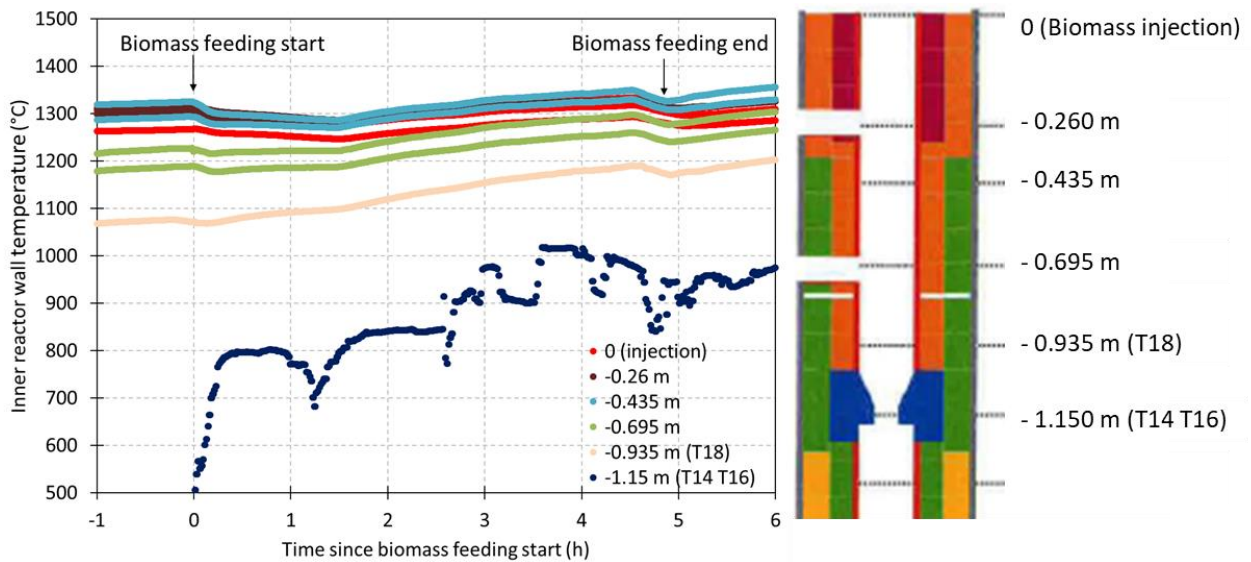


**Figure 2.** Temperatures measured as a function of time and position of the thermocouples along the upper part of the reactor

The temperatures measured at different heights are rather uniform along the reactor wall from the biomass injection zone down to 0.435 m from the injection level. At 0.695 m from the injection,

the temperature starts to be lower. The maximum temperature is around 1300-1350°C during biomass feeding. The power of the burner is increased from about 22 kW to 33 kW when biomass starts to be fed into the gasifier, in order to keep a constant temperature. However, the power is decreased at the end of the biomass injection period even if the temperature still increases due to the progressive decrease of the biomass feeding rate approaching the emptying of the lock-hoppers.

The maximum temperature measured in the cone level at 1.15 m from the injection level (T14 T16) is around 1000°C and around 1200°C at the level above (T18 0.935 m). The refractory along the reactor is a dense Al<sub>2</sub>O<sub>3</sub> in the upper part and a concrete Al<sub>2</sub>O<sub>3</sub>-SiO<sub>2</sub> refractory in the conical part (at 1.15 m from the injection level).

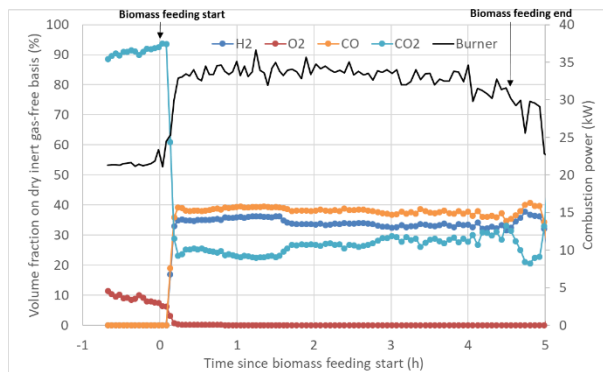


**Figure 3.** Dry inert gas-free gas composition as a function of time (major species) and combustion power of the burner

As expected, the main gaseous species during the biomass injection are H<sub>2</sub>, CO, H<sub>2</sub>O (not measured) and CO<sub>2</sub>. These are produced from the biomass thermochemical conversion, and are

mixed, or react, with CO<sub>2</sub> and H<sub>2</sub>O coming from the natural gas combustion. The H<sub>2</sub>/CO molar ratio is close to unity (0.9).

CH<sub>4</sub> content is comprised between about 0.5 and 1.5 %v, and is followed by C<sub>2</sub>H<sub>4</sub>, with a content ten times smaller than that of CH<sub>4</sub>, following the same variations. All the other gaseous species have a concentration under 0.05 %v.

These results obtained in an allothermal EFR reactor using a natural gas/O<sub>2</sub> burner are in agreement with literature<sup>11,12,13</sup> for such temperature range and biomass feedstocks obtained in an autothermal EFR reactor.

### **3.2 Residues and liquid characterizations**

About 1.9 kg dried residues (dry basis) were collected at the bottom of the EFR (**Figure 4**). Only a few grams of residues were collected on the filters at the exhaust of the EFR. Some traces were also observed on the windows at the top of the reactor.



**Figure 4.** Residues collected at the bottom of the EFR, exhaust and on windows

#### **3.2.1 Residues collected on the windows**

The residues collected on the windows were analyzed by SEM on graphite rubber (**Figure 5**).

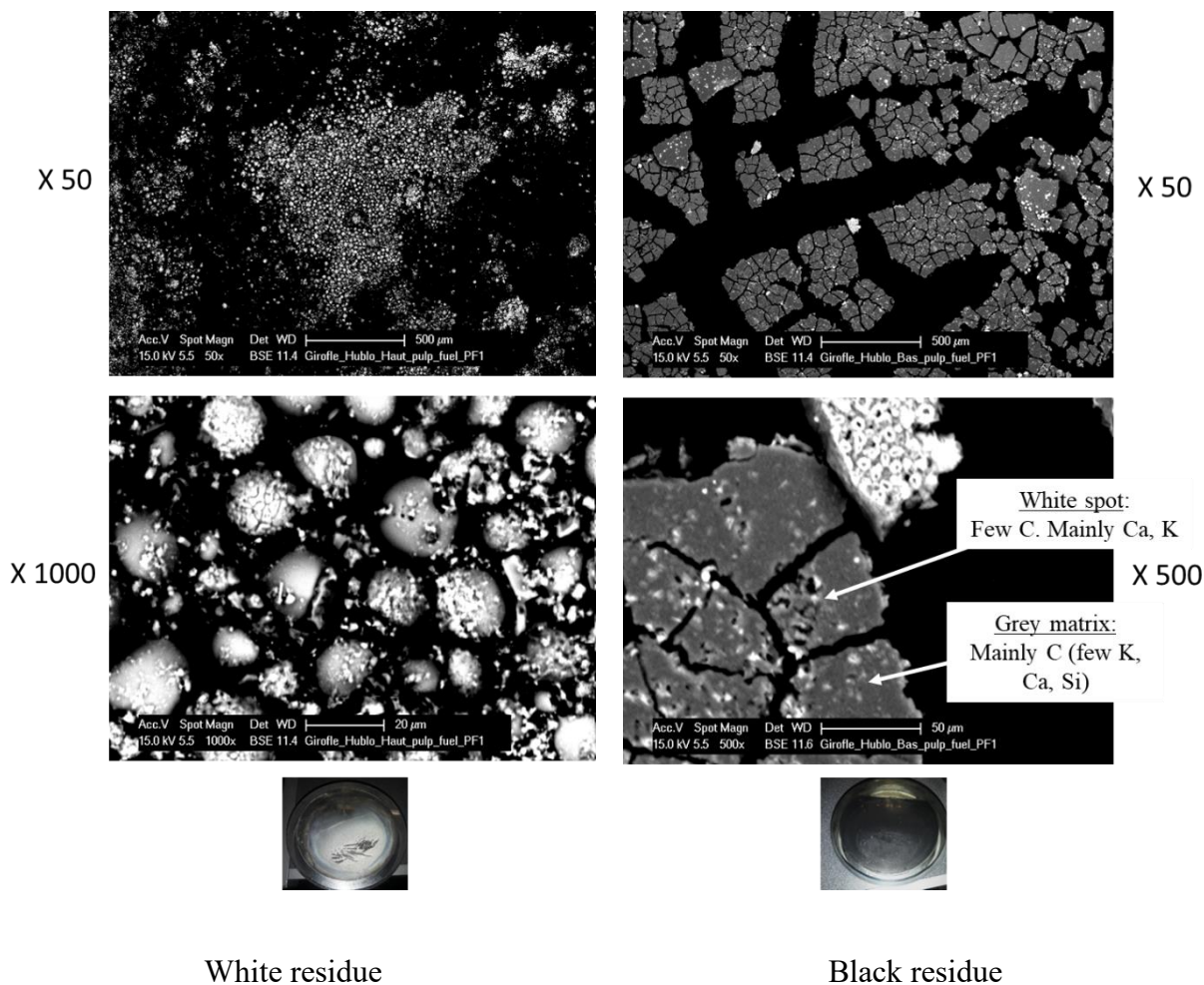


**Figure 5.** SEM-BSE on residues collected on windows (EDX shown in Supporting information Table S5)

The white residues observed on the top window are composed of spheres about 10  $\mu\text{m}$  in diameter, which are very rich in CaSiAlK, and look like silicate liquid droplets.

On the contrary, the black residues observed on the bottom window are mainly composed of unburned carbon or soots.

### **3.2.2 Residues collected in the filter at the exhaust of the reactor**

The residues collected on the filter were analyzed by SEM on graphite rubber (**Figure 6**).



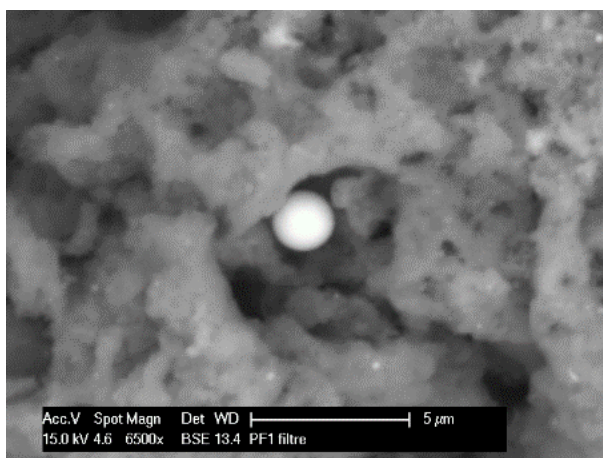


**Figure 6.** SEM BSE of residues collected in the filter

They are mainly constituted of carbon with some rare tiny glassy spheres (solidified slag).

### **3.2.3 Residues collected at the bottom of the reactor**

The residues collected at the bottom of the reactor were dried, weighed (1887g) and sieved in different classes (**Table 5**).

Residues (bottom EFR)	Mass fraction (wt %)	Ash yield (815°C) (wt %)
> 2500 μm	23	100*
630 – 2500 μm	9	42
100 – 630 μm	61	57

< 100 $\mu\text{m}$	7	57
---------------------	---	----

**Table 5.** Mass fraction and ash yield (815°C) in the different particle size classes (\*: not measured)

The particle size of the residue in the class 100 – 630  $\mu\text{m}$  has the higher mass fraction (61 wt%) and mainly corresponds to the initial particle size of the biomass. Only 23 wt% of the residues look like slag, mostly green (2/3) or black (1/3) (**Figure 7**).

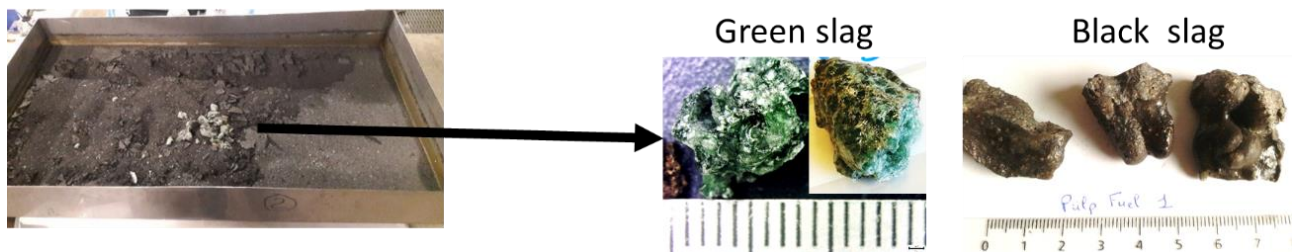


**Figure 7.** Residues collected after drying

The ash yield at 815°C was measured for each class of residue except the class >2500  $\mu\text{m}$  (**Table 5**). It is between 42 to 57 wt% indicating that some un-gasified carbon (650 g) was still present corresponding to 4.8 % of the introduced carbon. This means that more than 95 % of the introduced carbon has been gasified, which is very good.

The chemical composition of raw HW bark (turquoise) and each class of collected residues (orange and yellow) as well as the black and green slags (black and green respectively) are presented in **Figure 8**.

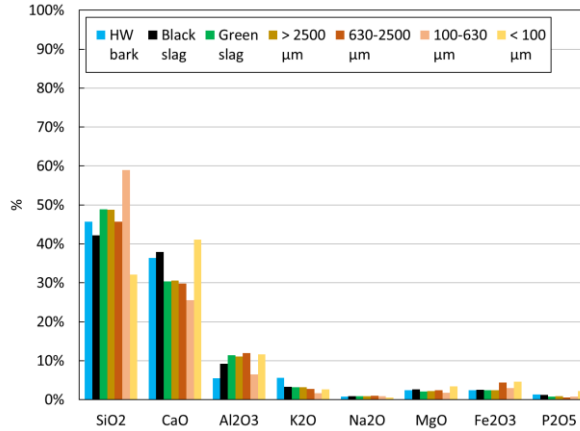
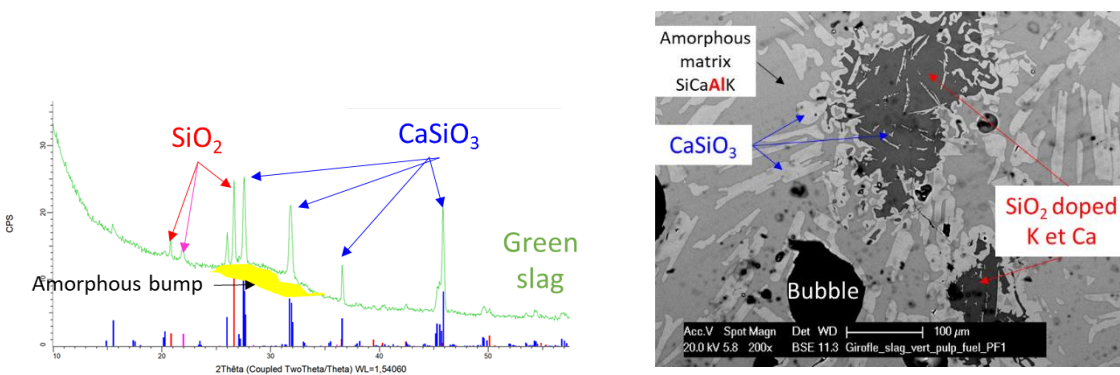


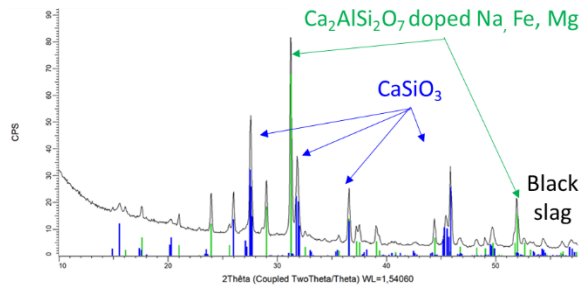
**Figure 8.** Chemical composition of raw HW bark and of collected residues in ash wt%

A clear increase of the alumina contents is observed for all the residues collected compared to the raw HW bark (in turquoise). The smaller class of slag (< 100 μm in yellow) is richer in CaO. The other classes are depleted in CaO (except the black slag) and K<sub>2</sub>O.

The green slag was characterized by P-XRD and SEM-EDS (**Figure 9-a and b**). The black slag and the residues < 100 μm and 100-630 μm were characterized by P-XRD only (**Figure 9-c**).



a- P-XRD diffractogram of the green slag



EDS (Wt%)	O	Na	Mg	Al	Si	P	K	Ca	Ti	Fe
SEM-EDS SiO <sub>2</sub> doped	45	0.8	1	2	34		7.5	7.5		1
SEM-EDS Amorphous matrix	43	0.8	1.7	6.5	22	0.5	3.5	19	0.2	2
ICP Green slag		0.7	1.3	6.2	23	0.4	2.7	22		1.7
ICP HW bark ash		0.5	1.3	2.6	19	0.5	4.2	23	0.1	1.5

b- SEM-EDS analysis of the green slag

c- P-XRD of the black slag

**Figure 9.** Characterization of black and green slags

An amorphous matrix (silicate liquid) with CaSiO<sub>3</sub> (wollastonite) and SiO<sub>2</sub> (quartz) - crystalline phases - is present in the green slag (**Figure 9-a and b**). A good agreement is observed between P-XRD and SEM-EDS. The amorphous phase composition is close to the global ICP measurements (slightly depleted in Si and Ca due to CaSiO<sub>3</sub> and SiO<sub>2</sub>). A pollution by alumina (probably coming from the reactor wall) is also observed. The large SiO<sub>2</sub> phase observed by SEM in the green slag sample seems to indicate some remaining silica pollution that may not be in equilibrium with the whole rest of the slag.

The black slag contains almost no amorphous (no liquid) and is much more crystallized with CaSiO<sub>3</sub> but also a lot of an alumino-silicate crystalline phase doped with Ca, Fe and Mg (gehlenite akermanite) (**Figure 9-c**). It seems to have solidified more slowly than the green slag allowing all phases to have time to crystallize, which may explain its black rather than green color. It could have stayed on the conical wall of the reactor before falling into the water. These green/black colored slags were also observed by Carlsson<sup>13</sup> with the same amorphous/crystallization P-XRD observations and higher alumina contamination of the black colored slag. The authors also deduced a different solidification path.

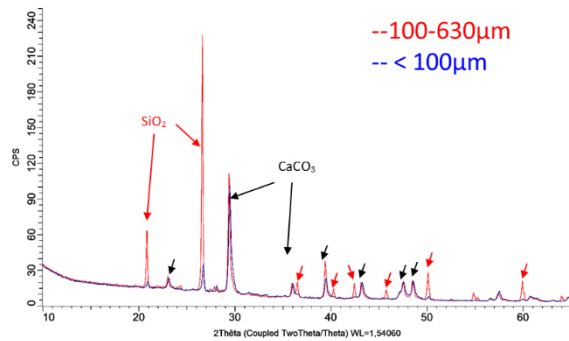


**Figure 10.** P-XRD on residues < 100  $\mu\text{m}$  (blue) and 100-630  $\mu\text{m}$  (red)

The amorphous phase (bump) and  $\text{CaSiO}_3$  (wollastonite) that were observed in the green slag are not observed in the smaller particles fraction (< 100  $\mu\text{m}$  and 100-630  $\mu\text{m}$ ) in **Figure 10**. For both fractions, the same crystalline phases  $\text{SiO}_2$  (quartz) and  $\text{CaCO}_3$  (calcite) are observed.

It is surprising to find  $\text{CaCO}_3$ . Indeed, if we reasonably assume that it is naturally present with  $\text{CaC}_2\text{O}_4$  (calcium oxalate) in a raw woody biomass<sup>3,27</sup>, the high temperatures encountered in the reactor (>1300°C) should have made it reacting with the other oxides of the feedstock (silicate and/or alkalis) or if in excess, should have decomposed it into  $\text{CaO}$  and  $\text{CO}_2(\text{g})$ . However  $\text{CaO}$  is not stable and, when cooled, will spontaneously, for one part, react to the high  $\text{CO}_2(\text{g})$  concentration in the syngas (several %v) and be converted to calcium carbonate ( $\text{CaCO}_3$ ), and for the other part, react with the water from syngas or quench and be converted to calcium hydroxide ( $\text{Ca}(\text{OH})_2$ ). These calcium oxides, when falling in the acidic water at the bottom of the reactor, are probably partly dissolved (see §3.2.4) and only calcium carbonate remains when the residue is collected and dried. Another explanation would be that, the residence time in the hot zone of the

reactor is too short for its decomposition/reaction with silicate and/or alkalis to have time to take place.

### 3.2.4 Water collected at the bottom of the reactor

The water collected at the bottom of the reactor was analyzed (**Table 6**). The total mass of water representative of the sampling was estimated to be 500 litres. This volume takes into account the maximum mass (volume) of water that remains in the reactor all along the test (450 litres) and the water coming from the burner during the biomass injection, from biomass gasification and from the water quench (~50 litres). The water produced during the heating of the reactor before the biomass injection (~200 litres) is not taken into account because this water overflows outside the reactor. The inorganic elements coming during the biomass injection are supposed to be dissolved in the full water present at the bottom of the reactor at the same time as water is overflowing.

	NH <sub>4</sub> <sup>+</sup>	Ca <sup>+</sup>	Mg <sup>+</sup>	K <sup>+</sup>	Na <sup>+</sup>	Cl <sup>-</sup>	NO <sub>3</sub> <sup>-</sup>	NO <sub>2</sub> <sup>-</sup>	SO <sub>4</sub> <sup>-</sup>	pH	Water collected
mg/l	<0.02	310	37	64	12	4	3190	0.23	<1	2.4	500 litres

**Table 6.** Anions, cations and pH measured in water collected at the bottom of the EFR

The main cations are Ca<sup>+</sup> and K<sup>+</sup> and the main anion is NO<sub>3</sub><sup>-</sup>. The pH is acidic. Carbonates (CO<sub>3</sub><sup>-</sup>) and hydrogenocarbonates (HCO<sub>3</sub><sup>-</sup>) anions were not measured. They should be very low with mainly CO<sub>2</sub>(g) dissolved in water due to the very acidic pH.

To explain the acidic pH and such a large amount of NO<sub>3</sub><sup>-</sup>, water was sampled just before the biomass injection and characterized in another test. An acidic pH and a very high concentration of NO<sub>3</sub><sup>-</sup> were also evidenced, with almost no other ionic species. This indicates that the high temperature and oxidizing gas of the natural gas/O<sub>2</sub> burner produce NO<sub>x</sub> from the injected N<sub>2</sub>.

Indeed, even when the biomass has not yet been injected, N<sub>2</sub> is injected to cool the end of the biomass supply system, which is located right next to the burner (**Figure 1**). Note that CO<sub>2</sub>(g) is also able to acidify the water, particularly in the first part of the test during the heating of the reactor by the natural gas/O<sub>2</sub> burner (CO<sub>2</sub>(g) ~ 25 %v).

The large amount of calcium dissolved in water can also be explained by the acidic water that favours calcium oxides dissolution.

### **3.3 Overall and elemental mass balance of ashes**

An overall mass balance was established for the ash by comparing (**Figure 11**):

- at the inlet, the theoretical mass of ash injected (1795 g) that is calculated with the total mass of dry biomass injected multiplied by its ash yield at 815°C (black circle in **Figure 11**).
- at the outlet, the mass of ash recovered at the bottom of the reactor (sum of ash mass from solid residue and from water soluble residue). The former (1237 g) is calculated using the dried collected residues for each sieved fraction multiplied by each ash yield at 815°C. The latter (522 g) shown as a green bar in **Figure 11** is calculated with the mass of water collected at the bottom of the EFR multiplied by the concentration in water (from ionic chromatography analyses) and considering that the inorganic elements are in the carbonate form.

The overall mass balance is well-closed (98 %). It is noteworthy that about 69 % of the ash mass is recovered in the solid residues and the rest - i.e. 29 % - is dissolved in the water. The smallest particles (< 100 µm) represent only 4 %. This class probably contains the fly ash (< 10 µm) because almost none is measured in the filter at the exhaust of the reactor.

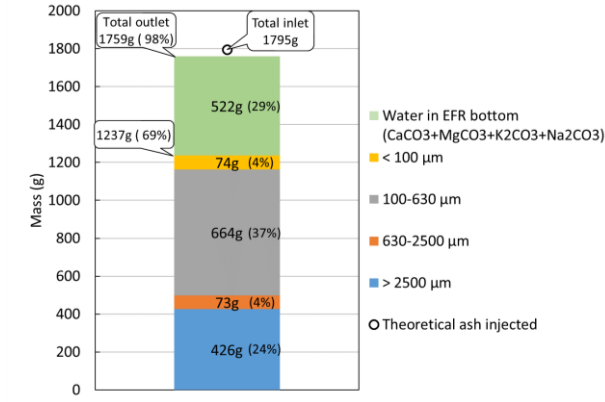


**Figure 11.** Overall mass balance of ashes

An elemental mass balance of ashes was done in the same way as the overall one for each inorganic element. All solid residues were analyzed by ICP and the water was analyzed by ionic chromatography (**Figure 12**).

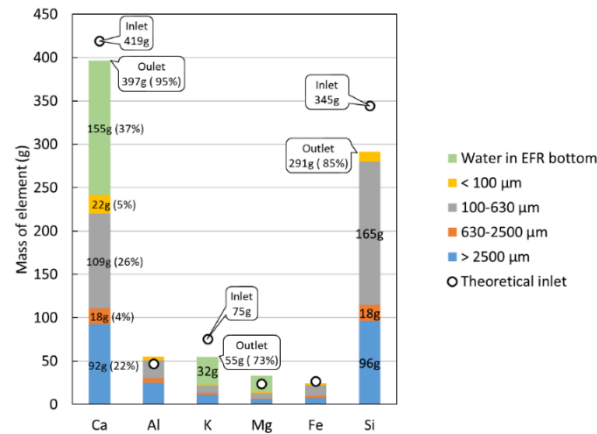


**Figure 12.** Elemental mass balance of ashes

The elemental mass balance is only shown for the elements that were introduced into the reactor with a mass high enough (i.e. > 10 g) to have a chance to be recovered in the reactor. Elements S, Cl, Na and P are thus not shown. Neither is N shown, even if its inlet mass is high (97 g), because there is almost four times more N measured in the water than introduced into the reactor, due to N<sub>2</sub> oxidized to NO<sub>x</sub> in the burner flame and then dissolved in the water (see § 3.2.4).



However, the mass balance is still done anyway for S (inlet mass = 8.3 g) because H<sub>2</sub>S and COS were clearly measured by  $\mu$ GC at the exhaust of the reactor giving 72 % recovered, which is not an odd result. S recovered in slags was 5 % and less than 1 % in the water. The total mass balance of S is thus calculated to be 77 % S, which is not too bad.

For the two main elements (Ca, Si), the mass balance is almost closed (95 %, 85 %). Ca is the main element soluble in acidic water. Some Mg and K were also dissolved. The missing Si, Ca and K elements in the mass balance are probably left in the slag stuck on the wall reactor.

The quite high amount of K soluble in the water (~ 44 %) is not mainly coming from KCl nor K<sub>2</sub>SO<sub>4</sub> because a very small amount of Cl<sup>-</sup> and SO<sub>4</sub><sup>-</sup> is recovered in the water. This is in agreement with quench effluents measurements during bark gasification in EFR.<sup>12</sup> It must be due to some KOH(g) and/or K(g) soluble in water as predicted by thermodynamic equilibrium calculations.<sup>28</sup>

The attempt to calculate the Cl recovered in the water is 29 % (2 g over 6.9 g inlet). Cl was not measured in the solid residues and not detected by P-XRD. No conclusion can be drawn.

Note that the Mg and Fe inlet amounts are too small (~ 20 g) to really conclude. It is not the case for Al introduced in a higher amount (~ 50 g inlet). A higher amount of Al was collected at the outlet than introduced with the feedstock, confirming the slight alumina pollution by the reactor wall.

### **3.4 Simulation tools and comparison with experiments**

#### **3.4.1 Thermodynamic calculations using phase diagram**

The phase diagram of the three main oxides of HW bark ashes (SiO<sub>2</sub>-CaO-K<sub>2</sub>O) calculated at 1300 and 1400°C is shown in **Figure 13**. The temperature of the tests is closer to 1300 rather than

1400°C (**Figure 2**). The green, white and red colored areas correspond to 100% solid, solid + liquid and 100% liquid as explained in De Fusco<sup>29</sup> to better understand these isothermal sections of the phase diagrams. The liquidus temperature is the boundary line between the liquid and solid + liquid area (boundary between white and red areas). When the temperature is increased from 1300 to 1400°C the liquid area is obviously increased.

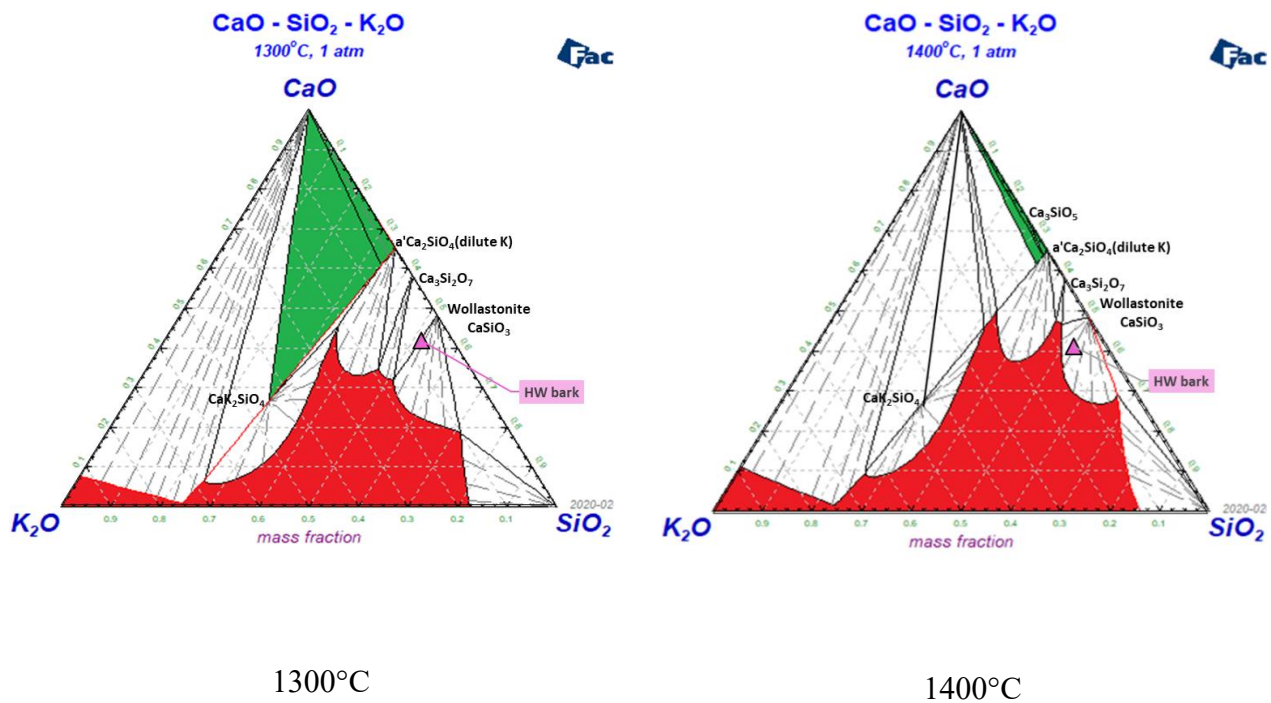


**Figure 13.** SiO<sub>2</sub>-CaO-K<sub>2</sub>O phase diagram calculated with Factsage 7.3 and the database FToxid7.3

The HW bark ash composition is plotted (pink triangle) in **Figure 13** at 1300 and 1400°C. It is predicted to be solid (CaSiO<sub>3</sub>) + liquid even at 1400°C. These results are in agreement with the phases observed by P-XRD for the black and green slags characterized previously.

### 3.4.2 Thermodynamic calculations using global calculations

The previous conclusions were obtained by analyzing only the three main oxides. A small content of other elements could change the phase behavior. Global calculations were conducted with all the elements of HW bark and taking into account the atmosphere and total pressure. The assumptions and initial mass balance are reported in **Supporting information (Table S2 to S4)**.

**Figure 14** shows the prediction of the effect of temperature in the nature of the condensed phases (solid + liquid).

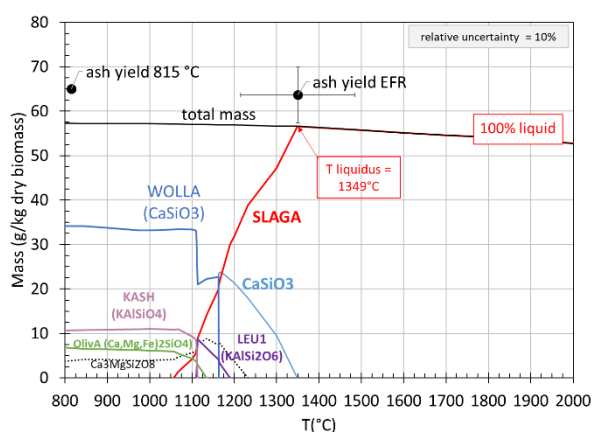


**Figure 14.** Mass of condensed phases predicted (g/kg dry biomass) (lines) and of measured ash yield at 815°C and ash yield of the EFR test (black round dots). A typical relative uncertainty of 10% is shown

It is observed that the solidus temperature - i.e. apparition of the liquid phase (called SLAGA) - is calculated at 1043 °C and the liquidus temperature - i.e. disappearance of any solid phase - is calculated at 1349°C.

The main solid phase in equilibrium with the liquid phase is  $\text{CaSiO}_3$  (Wollastonite) in the whole range of temperatures. This is in agreement with the phase diagrams approach with the three main

oxides (**Figure 13**). These predictions are in agreement with the P-XRD results collected on the large particle size residues ( $> 2500 \mu\text{m}$  i.e. black and green slag).

Other phases in smaller quantity such as a Ca-Mg silicate ( $\text{Ca}_3\text{MgSi}_2\text{O}_8$ ) and some K-Al-silicates ( $\text{KAlSi}_2\text{O}_6$  (Leucite) and  $\text{KAlSiO}_4$  (Kalsilite)) are predicted to appear at lower temperatures. They are not observed by P-XRD probably because in too small amount or due to the solidification pathway. Instead, the crystalline phase  $\text{SiO}_2$  (quartz) is observed by P-XRD for the green slag along with a doped  $\text{Ca}_2\text{AlSi}_2\text{O}_7$  (melilite) for the black slag.

The smaller class of residues ( $< 630 \mu\text{m}$ ) is composed of  $\text{SiO}_2$  and  $\text{CaCO}_3$  that are not predicted.

The total mass of the condensed phase is calculated between 57 g at  $800^\circ\text{C}$  and 53 g at  $2000^\circ\text{C}$  close to the experimental ash yield measured at  $815^\circ\text{C}$  in air and from the mass balance in the EFR (65 g and 62 g per kg db respectively).

The volatilization of each element is calculated in **Figure 15**. The main gaseous species involved are shown in parenthesis.

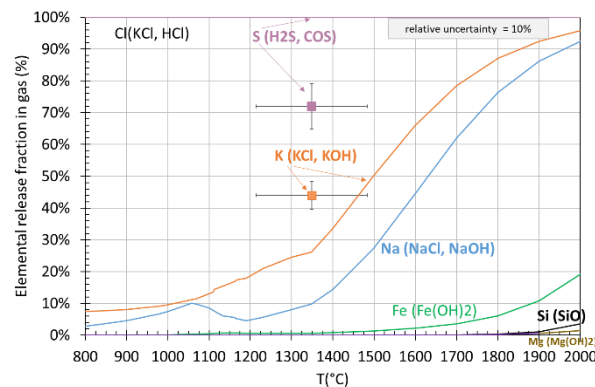


**Figure 15.** Elemental volatilization predicted (lines) and measured (square dots). A typical relative uncertainty of 10 % is shown

A full volatilization of S (as H<sub>2</sub>S and COS) and Cl (as KCl and HCl) is calculated from 800°C. Comparison with experimental results is uncertain because these elements are introduced into the reactor with a mass (i.e. 8.3 g S and 6.9 g Cl) too low to have a chance to be recovered in the reactor. However, some H<sub>2</sub>S and COS are clearly measured by μGC showing that 72% of S is in the gas phase, which is the good tendency predicted.

In the temperature range of the EFR test (1000–1400°C) about 10 to 30% of the initial K (as KCl, KOH) and about 10% of Na (as NaCl, NaOH) are predicted to be released in the gas phase. The measure of the volatilized K is taken from the K soluble in water after being released in the gas phase. The unknown mass of K in **Figure 15** was taken into account by distributing it over all the measurements (gases, solids). It is measured at 44%, which is a little higher than predicted.

The composition of the liquid phase (SLAGA) is plotted in wt% versus the temperature in **Figure 16-a**.

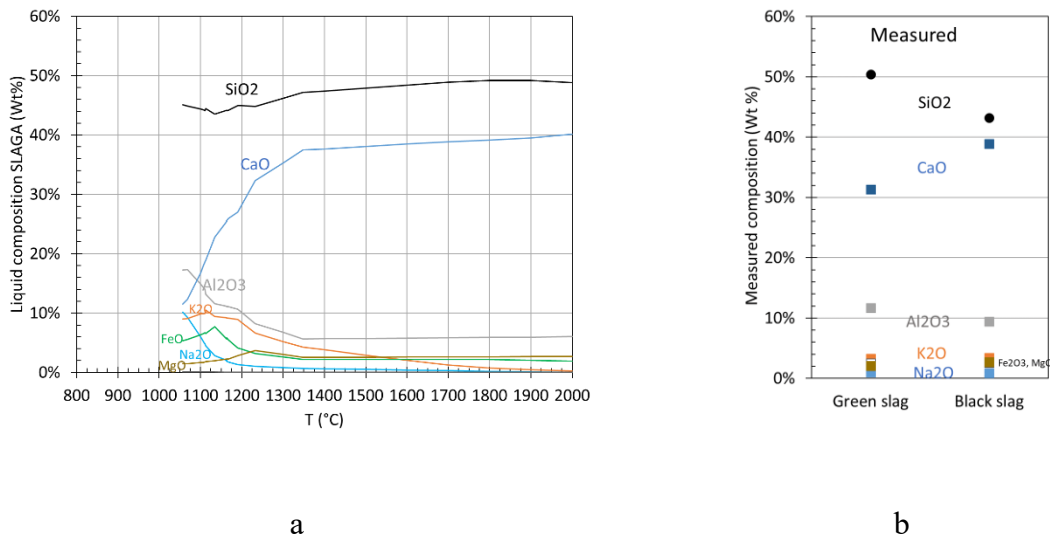


**Figure 16.** Composition of the liquid phase predicted (a) and measured (b)

The liquid phase is predicted to be rich in  $\text{SiO}_2$ , then  $\text{CaO}$ ,  $\text{Al}_2\text{O}_3$  and  $\text{K}_2\text{O}$ . When the temperature increases,  $\text{CaO}$  strongly increases due to the dissolution of the Ca rich condensed phases which cause the decrease of the other oxides by dilution effect. Above the liquidus temperature of  $1348^\circ\text{C}$ ,  $\text{K}_2\text{O}$  is decreasing due to the K volatilization as  $\text{KOH}(\text{g})$  and  $\text{K}(\text{g})$ . The measured composition of the green and black slags is shown by comparison in **Figure 16-b**. The green slag composition measure is close to the  $1200^\circ\text{C}$  calculated one, except that of  $\text{K}_2\text{O}$  which is measured lower. This may be due to the volatility of K which is measured slightly higher than that calculated (**Figure 15**). The black slag does not fit with any temperature.

To try explaining the black slag composition and its Ca-Al silicate (melilite) observed by P-XRD, the effect of the interaction between the ashes and the ceramic refractory materials of the reactor wall - dense alumina in the upper part and refractory concrete ( $60\% \text{Al}_2\text{O}_3$ - $40\% \text{SiO}_2$ ) in the lower conical part - is also calculated at  $1150^\circ\text{C}$ . The main calculated condensed phases are shown in **Figure 17**.

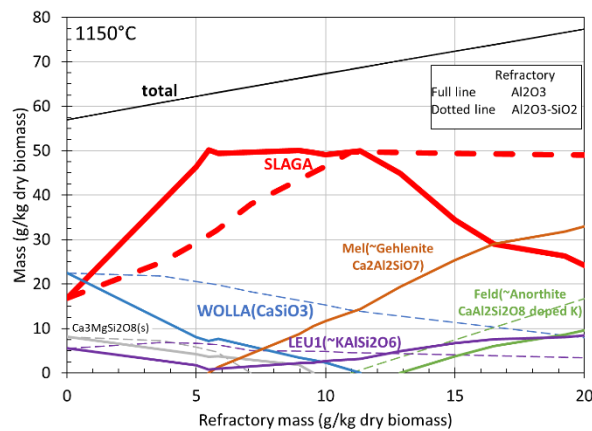


**Figure 17.** Mass of condensed phases when ashes are in interaction with  $\text{Al}_2\text{O}_3$  (full line) or  $\text{Al}_2\text{O}_3$ - $\text{SiO}_2$  (dotted line) predicted (g/kg dry biomass)

Both refractories have fully reacted - i.e. no excess of  $\text{Al}_2\text{O}_3$  nor  $\text{Al}_2\text{O}_3\text{-SiO}_2$  remains at equilibrium - up to 20 g/kg db of the refractory. They firstly dissolved in the liquid phase SLAGA whose amount increased with the increased amount of refractory. The liquid phase increased faster for the dense alumina rather than with the refractory concrete and stabilized after reacting with 5.5 g of  $\text{Al}_2\text{O}_3$  (11 g of  $\text{Al}_2\text{O}_3\text{-SiO}_2$ ).

When the solubility limit is reached, a new solid phase rich in alumina appears (gehlenite  $\text{Ca}_2\text{Al}_2\text{SiO}_7$  for  $\text{Al}_2\text{O}_3$  and anorthite  $\text{CaAl}_2\text{SiO}_8$  for  $\text{Al}_2\text{O}_3\text{-SiO}_2$ ). Both phases are Ca-Al silicates as it is observed for the black slag by P-XRD.

The composition of the liquid phase (SLAGA) is reported in **Figure 18**.

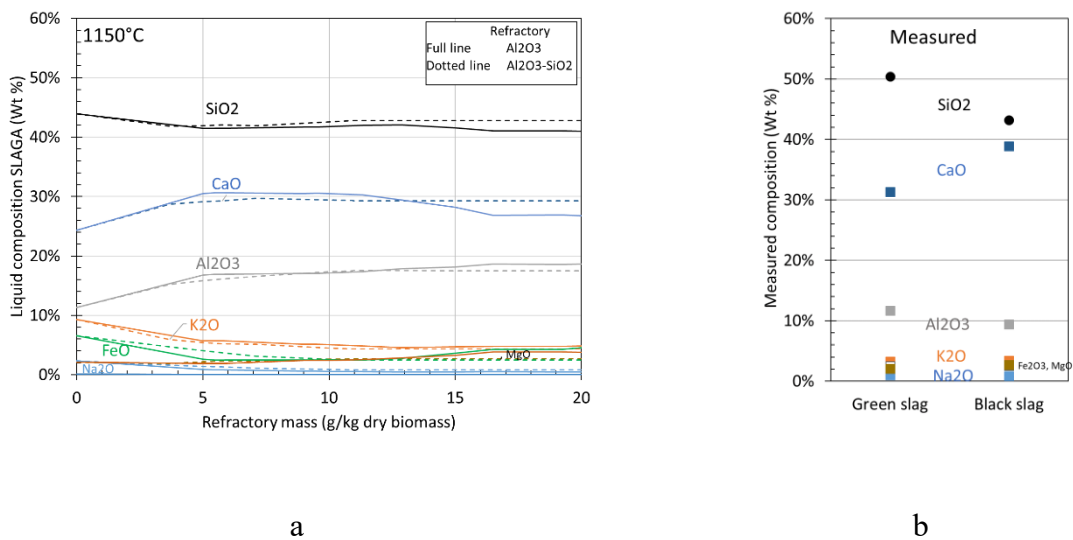


**Figure 18.** Composition of the liquid phase predicted when ashes are in interaction with  $\text{Al}_2\text{O}_3$  (full line) or  $\text{Al}_2\text{O}_3\text{-SiO}_2$  (dotted line) (a) and measured (b) (same Figure than 16-b)

The same composition is observed whatever the refractory dissolution (slightly higher silica for the refractory  $\text{Al}_2\text{O}_3 - \text{SiO}_2$ ). When the mass of the refractory increases, the compositions in  $\text{Al}_2\text{O}_3$  and  $\text{CaO}$  increase, and those in  $\text{K}_2\text{O}$  and  $\text{SiO}_2$  decrease.

When comparing the calculated composition of the liquid phase (**Figure 18-a**) with the measured one for the black slag (**Figure 16-b**), a better agreement is observed within the alumina contents for both slags. However, a higher calcia content is measured.

### **3.4.3 Thermodynamic calculations: discussion**

These results show a good consistency between experimental results collected on the large particle size residues ( $> 2500 \mu\text{m}$  i.e. black and green slag) and the prediction either from simple phase diagram or with global calculations. In this case, the effect of the other elements does not change the prediction of the main solid phases in equilibrium with the liquid.

Carlsson<sup>13</sup> found that its global calculations with Factsage 6.4 could not adequately reproduce its measurements (slag composition and K volatilization) which is in contradiction with the good reproducibility we observed with our experiments. The more recent database we used is not the reason of this contradiction. In fact, Carlsson's fuel and ours are very different even though they both come from woody biomass. Carlsson's fuel is a clean woody biomass whose composition is  $\text{SiO}_2$ -poor. On the contrary, we used a hard wood bark polluted by soil whose composition is in the  $\text{SiO}_2$ -rich part of the  $\text{SiO}_2$ - $\text{CaO}$ - $\text{K}_2\text{O}$  phase diagram (**Figure 13**). It is possible that our prediction is closer to the measurements because the  $\text{SiO}_2$ -rich part of the ternary phase diagram is best known.<sup>30</sup> Another explanation could be to take into account the interaction between the ashes and the refractory in the input of Carlsson's global calculation. We performed this simulation using their inputs and found that the solidus temperature decreased strongly, K was trapped in the



liquid slag and its volatility decreased. These predictions are then closer to Carlsson's experimental findings. Carlsson<sup>13</sup> and Ma<sup>31</sup> proposed a more complex scheme in several calculations steps including the fractionation between the gas and the condensed phase of the ash. Our results show that it is not necessary to perform such refined calculations to reproduce the experimental results.

The effect of a silica rich biomass or a woody biomass polluted by silica was already pointed out by Ma<sup>11,12</sup> to favor the melt formation and its strong interaction with the refractory wall. Our experimental results do not show such a strong interaction of the ash with the refractory material.

However it is noteworthy that the good consistency between experimental and predicted results were obtained for the larger particle size residues (> 2500  $\mu\text{m}$  i.e. black and green slag) corresponding only to 24 wt% (**Figure 11**) of the collected residues instead of 100 wt% of the total ash mass as predicted in **Figure 14**. The rest of the ashes - i.e. about 70 wt%, consisting in the smaller class of residues (< 630  $\mu\text{m}$ ) and of the ash dissolved in the water quench - is composed of  $\text{SiO}_2$  and  $\text{CaCO}_3$ , which was not predicted by calculations. This shows that a large amount of the ash (~70 wt%) does not seem to be in thermodynamic equilibrium. It seems that a part of the soil ( $\text{SiO}_2$ ) and of the compounds ( $\text{CaO}$ ,  $\text{CaCO}_3$ ,  $\text{CaC}_2\text{O}_4$ ,  $\text{KCl}$ , etc.) initially present in the raw HW bark<sup>3,27</sup> did not react together to give  $\text{CaSiO}_3$  and the liquid phase.

Then it seems that one global calculation is sufficient to get reliable results for the slag composition and K volatilization. This global calculation takes into account the ash fractionation and the chemical reaction between the refractory wall and the gas and the ashes. However it is possible that only a part of the silica from soil reacted with the other native elemental form of the woody biomass or with the refractory due to kinetic or hydrodynamic reasons.

### 3.4.4 Viscosity calculations

Prediction of the viscosity of the ashes are shown in **Figure 19** from the composition of the liquid phase calculated at equilibrium with Factsage (red line) and from measurements of the composition of the black (black line) and green (green line) slags. For the slag to flow along the reactor wall, it is generally accepted that the slag viscosity must be sufficiently low at the temperature of tapping, typically less than 10 - 25 Pa s (arrow represented in **Figure 19**).<sup>32</sup>

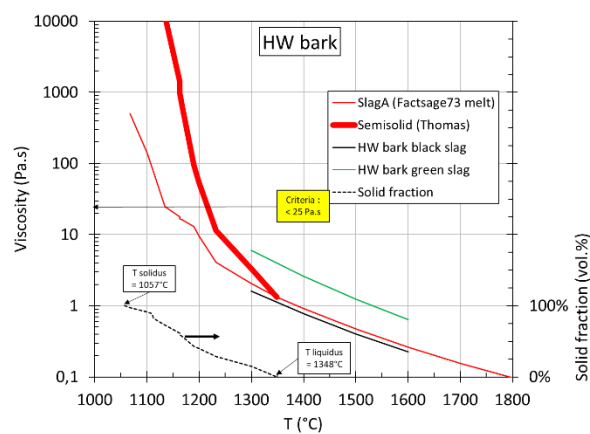


**Figure 19.** Viscosity calculations of the HW bark ashes (lines) and volumetric solid fraction calculated with Factsage (dotted line)

Above the predicted liquidus temperature ( $> 1348^{\circ}\text{C}$ ) the viscosity calculated from the calculated liquid composition or from the measured black and green slags compositions is less than 10 Pa.s.

Below the liquidus temperature, due to the solid fraction increasing, the viscosity is sharply increasing and reaches a viscosity higher than 25 Pa.s for a temperature below  $\sim 1200^{\circ}\text{C}$  (Thomas's model prediction).

The maximum temperature measured at the level of the cone (T14 T16 -1.15 m **Figure 2**) is around  $1000^{\circ}\text{C}$  and around  $1200^{\circ}\text{C}$  at the level above (T18 – 0.935 m **Figure 2**). Both slags collected

(black or green) looked glassy like solidified silicate liquid (**Figure 7**) even if the black slag seemed to be more crystallized by P-XRD because a slower solidification. Taking into account all the uncertainties in the viscosity calculations and in the temperature gradient, these calculations are in qualitative agreement with the fact that the slags collected probably flowed along the bottom of the reactor wall.

These viscosity calculations do not agree with the results found by Ma<sup>12,13</sup> regarding their bark wood and their wood. Their viscosities were much higher ( $> 10^4$  Pa.s) for temperatures less than 1350°C. As already pointed out, the main reason is the composition of the HW bark of our study which is much richer in silica (due to soil pollution) than their bark wood.<sup>12</sup> The solidus/liquidus temperatures of the HW bark are thus lower ( $\sim 100^\circ\text{C}$ ) than those of their bark wood (1057/1348°C versus 1140/1480°C). The influence of the solid fraction increases strongly the viscosity in the working EFR temperature range (1250-1350°C) of their bark wood. The viscosity is known to be higher for SiO<sub>2</sub>-rich liquid. Nevertheless, the effect of the solid fraction in a SiO<sub>2</sub>-poor liquid is also very effective in increasing the viscosity.

#### **4. CONCLUSION**

HW bark was gasified on a pilot scale in a pressurized slagging EFR (250 KWth) in allothermal conditions, with a 6 kg/h feeding rate during 5 hours, a total pressure of 5 bars and a maximum wall temperature of 1300-1350°C. Consistent results were obtained for the gas composition. No blockage linked to the ash/slag was observed even though about 1.8 kg of the theoretical ash mass was injected. More than 95% of the carbon from the biomass was converted into gas species.

About 1.9 kg of dried residues were collected at the bottom of the reactor corresponding to 1.3 kg of ash and 0.6 kg of unburned carbon. A high amount of ashes were dissolved in the water quench

mainly as Ca and K cations. A high amount of  $\text{NO}_3^-$  anions were also measured in the water quench coming from the oxidation of the introduced  $\text{N}_2$  gas (and not from the N-biomass) in the high temperature zone of the  $\text{O}_2/\text{CH}_4$  burner, and were mainly responsible for the acidic pH. The overall ash and (Ca, K, Si) mass balances were both well closed.

Predictive calculation at equilibrium of the main condensed phases - i.e.  $\text{CaSiO}_3$  and liquid (amorphous) - were in agreement with the P-XRD observations for only 1/4 of the collected ashes. The remaining ashes (3/4) were composed of phases that were not predicted by calculations:  $\text{SiO}_2$  probably from soil and of  $\text{CaCO}_3$  from compounds initially present in the raw HW bark. This shows that only a part of the polluted soil reacted with the raw HW bark ash. A slight pollution by the alumina wall of the reactor was observed and confirmed by calculations. A very small amount (< 4%) of fly ashes were noticed.

Viscosity calculations are below the criteria of 25 Pa.s in the temperature range of the test.

## **5. AUTHOR INFORMATION**

Corresponding Author: Françoise Defoort (francoise.defoort@cea.fr)

### Author Contributions

The manuscript was written through contributions of all the authors. All the authors have given approval to the final version of the manuscript.

## **6. ACKNOWLEDGMENTS**

This work has received funding from the European Union's Horizon H2020 research and innovation program under grant agreement number 818011. The French ANR (French Agency for research) is also acknowledged for having partly funded the GIROFLE entrained flow reactor

within the framework of EQUIPEX 2011 equipment of excellence of the Future Investments Program.

## **7. ASSOCIATED CONTENT**

**Supporting informations** are available free of charge. They contain the list of solutions taken into account for the thermodynamic calculations with the Factsage software (Table S1) as well as the initial mass balance to perform the calculations (Table S2 to S4) and an example of Factsage results (§3). Some EDX semi quantification of residues collected on the top and bottom of the EFR windows are presented in Table S5.

## 8. REFERENCES

- (1) Wang, P.; Massoudi, M. Slag Behavior in Gasifiers. Part I: Influence of Coal Properties and Gasification Conditions. *Energies* **2013**, *6* (2). <https://doi.org/10.3390/en6020784>.
- (2) Van der Drift, A.; Boerrigter, H.; Coda, B.; Cieplik, M. K.; Hemmes, K. [ECN B., Petten (Netherlands)]. *Entrained Flow Gasification of Biomass. Ash Behaviour, Feeding Issues, System Analyses*; Netherlands, 2004.
- (3) Vassilev, S. V.; Baxter, D.; Andersen, L. K.; Vassileva, C. G. An Overview of the Chemical Composition of Biomass. *Fuel* **2010**, *89*, 913–933.
- (4) Coda, B.; Cieplik, M. K.; de Wild, P. J.; Kiel, J. H. A. Slagging Behavior of Wood Ash under Entrained-Flow Gasification Conditions. *Energy & Fuels* **2007**, *21*, 3644–3652.
- (5) Leiser, S.; Cieplik, M. K.; Smit, R. Slagging Behavior of Straw and Corn Stover and the Fate of Potassium under Entrained-Flow Gasification Conditions. *Energy Fuels* **2013**, *27* (1), 318–326. <https://doi.org/10.1021/ef301821a>.
- (6) Qin, K.; Lin, W.; Fæster, S.; Jensen, P. A.; Wu, H.; Jensen, A. D. Characterization of Residual Particulates from Biomass Entrained Flow Gasification. *Energy Fuels* **2013**, *27* (1), 262–270. <https://doi.org/10.1021/ef301432q>.
- (7) Bläsing, M.; Müller, M. Release of Alkali Metal, Sulfur, and Chlorine Species during High-Temperature Gasification of Coal and Coal Blends in a Drop Tube Reactor. *Energy & Fuels* **2012**, *26*, 6311–6315. <https://doi.org/10.1021/ef301205j>.
- (8) De Fusco, L.; Blondeau, J.; Defoort, F.; Jeanmart, H.; Contino, F. Characterization of Sunflower Husks Fouling in a Drop Tube Furnace: Comparison of Deposits with H<sub>3</sub>PO<sub>4</sub>, CaCO<sub>3</sub> and Al<sub>2</sub>Si<sub>2</sub>O<sub>5</sub>(OH)<sub>4</sub> Additives. In *European Biomass Conf. Exhib. Proc.*; ETA-Florence Renewable Energies, 2016; Vol. 2016, pp 748–755.
- (9) Wagner, D. R.; Holmgren, P.; Skoglund, N.; Broström, M. Design and Validation of an Advanced Entrained Flow Reactor System for Studies of Rapid Solid Biomass Fuel Particle Conversion and Ash Formation Reactions. *Rev. Sci. Instrum.* **2018**, *89* (6). <https://doi.org/10.1063/1.5030603>.
- (10) Holmgren, P.; Broström, M.; Backman, R. Slag Formation during Entrained Flow Gasification: Silicon-Rich Grass Fuel with a KHCO<sub>3</sub> Additive. *Energy Fuels* **2018**, *32* (10), 10720–10726. <https://doi.org/10.1021/acs.energyfuels.8b02545>.
- (11) Ma, C.; Weiland, F.; Hedman, H.; Boström, D.; Backman, R.; Öhman, M. Characterization of Reactor Ash Deposits from Pilot-Scale Pressurized Entrained-Flow Gasification of Woody Biomass. *Energy & Fuels* **2013**, *27*, 6801–6814.
- (12) Ma, C.; Carlborg, M.; Hedman, H.; Wennebro, J.; Weiland, F.; Wiinikka, H.; Backman, R.; Öhman, M. Ash Formation in Pilot-Scale Pressurized Entrained-Flow Gasification of Bark and a Bark/Peat Mixture. *Energy & Fuels* **2016**, *30*, 10543–10554.
- (13) Carlsson, P.; Ma, C.; Molinder, R.; Weiland, F.; Wiinikka, H.; Öhman, M.; Öhrman, O. Slag Formation during Oxygen-Blown Entrained-Flow Gasification of Stem Wood. *Energy Fuels* **2014**, *28* (11), 6941–6952. <https://doi.org/10.1021/ef501496q>.
- (14) Seebold, S.; Eberhard, M.; Wu, G.; Yazhenskikh, E.; Sergeev, D.; Kolb, T.; Müller, M. Thermophysical and Chemical Properties of Bioliq Slags. *Fuel* **2017**, *197*, 596–604.
- (15) Cavagnol, S. M.; Covella, K.; Müller-Hagedorn, M. Determination of Slag Deposition Rate on Cooling Screen Reactor Walls by Utilisation of Slag Thickness Measurements. *Fuel* **2018**, *228*, 369–378. <https://doi.org/10.1016/j.fuel.2018.04.089>.

- (16) Dahmen, N.; Abeln, J.; Eberhard, M.; Kolb, T.; Leibold, H.; Sauer, J.; Stapf, D.; Zimmerlin, B. The Bioliq Process for Producing Synthetic Transportation Fuels. *WIREs Energy Environ* **2017**, *6* (3), 1 to 10. <https://doi.org/10.1002/wene.236>.
- (17) Jung, I.-H.; Van Ende, M.-A. Computational Thermodynamic Calculations: FactSage from CALPHAD Thermodynamic Database to Virtual Process Simulation. *Metallurgical and Materials Transactions B* **2020**, *51* (5), 1851–1874. <https://doi.org/10.1007/s11663-020-01908-7>.
- (18) Seiler, J.-M. CEA Research Activities in the Field of Entrained Flow Reactors, 2007, 8-12 may, 2nd Int. Freiberg Conf. On IGCC and XtL technologies.
- (19) Urbain, G. Viscosity Estimation of Slags. *Steel Research* **1987**, *58*, 111–116.
- (20) Bale, C. W.; Belisle, E.; Chartrand, P.; Decterov, S. A.; Eriksson, G.; Hack, K.; Jung, I. H.; Kang, Y. B.; Melancon, J.; Pelton, A. D.; Robelin, C.; Petersen, S. FactSage Thermochemical Software and Databases - Recent Developments. *Calphad: Computer Coupling of Phase Diagrams and Thermochemistry* **2009**, *33*, 295–311.
- (21) Duchesne, M. A.; Bronsch, A. M.; Hughes, R. W.; Masset, P. J. Slag Viscosity Modeling Toolbox. *Fuel* **2013**, *114*, 38–43. <https://doi.org/10.1016/j.fuel.2012.03.010>.
- (22) Wu, G.; Seebold, S.; Yazhenskikh, E.; Tanner, J.; Hack, K.; Müller, M. Slag Mobility in Entrained Flow Gasifiers Optimized Using a New Reliable Viscosity Model of Iron Oxide-Containing Multicomponent Melts. *Applied Energy* **2019**, *236*, 837–849. <https://doi.org/10.1016/j.apenergy.2018.11.100>.
- (23) Thomas, D. G. Transport Characteristics of Suspension .8. a Note on Viscosity of Newtonian Suspensions of Uniform Spherical Particles. *Journal of Colloid Science* **1965**, *20*, 267-.
- (24) Kondratiev, A.; Ilyushechkin, A. Flow Behaviour of Crystallising Coal Ash Slags: Shear Viscosity, Non-Newtonian Flow and Temperature of Critical Viscosity. *Fuel* **2018**, *224*, 783–800. <https://doi.org/10.1016/j.fuel.2018.03.031>.
- (25) Mills, K. C.; Rhine, J. M. The Measurement and Estimation of the Physical Properties of Slags Formed during Coal Gasification: 1. Properties Relevant to Fluid Flow. *Fuel* **1989**, *68* (2), 193–200. [https://doi.org/10.1016/0016-2361\(89\)90322-0](https://doi.org/10.1016/0016-2361(89)90322-0).
- (26) Lange, R. A. A Revised Model for the Density and Thermal Expansivity of K<sub>2</sub>O-Na<sub>2</sub>O-CaO-MgO-Al<sub>2</sub>O<sub>3</sub>-SiO<sub>2</sub> Liquids from 700 to 1900 K: Extension to Crustal Magmatic Temperatures. *Contributions to Mineralogy and Petrology* **1997**, *130* (1), 1–11.
- (27) Werkelin, J.; Skrifvars, B.-J.; Zevenhoven, M.; Holmbom, B.; Hupa, M. Chemical Forms of Ash-Forming Elements in Woody Biomass Fuels. *Fuel* **2010**, *89* (2), 481–493. <https://doi.org/10.1016/j.fuel.2009.09.005>.
- (28) Froment, K.; Defoort, F.; Bertrand, C.; Seiler, J. M.; Berjonneau, J.; Poirier, J. Thermodynamic Equilibrium Calculations of the Volatilization and Condensation of Inorganics during Wood Gasification. *Fuel* **2013**, *107*, 269–281. <https://doi.org/10.1016/j.fuel.2012.11.082>.
- (29) De Fusco, L.; Defoort, F. A Thermochemical Approach Based on Phase Diagrams to Characterize Biomass Ash and Select the Optimal Thermal Conversion Technology. In *6th International Symposium on Energy from Biomass and Waste*; Venise, Italie, 2016.
- (30) Morey, G.; Kracek, F. C.; Bowen, N. L. The Ternary System K<sub>2</sub>O-CaO-SiO<sub>2</sub>. *J. Soc. Glass. Technol.* **1930**, *14*, 149.

- (31) Ma, C.; Backman, R.; Ohman, M. Thermochemical Equilibrium Study of Slag Formation during Pressurized Entrained-Flow Gasification of Woody Biomass. *Energy & Fuels* **2015**, *29*, 4399–4406.
- (32) Hoy, H.; Roberts, A.; Wilkins, D. *Behaviour of Mineral Matter in Slagging Gasification Process*; Institution of Gas Engineers, 1964.



# TOC graphic

